Article

Analysis of Favourable Process Conditions for the Manufacturing of Thin-Wall Pieces of Mild Steel Obtained by Wire and Arc Additive Manufacturing (WAAM)

José Luis Prado-Cerqueira [1], Ana María Camacho [1], José Luis Diéguez [2], Álvaro Rodríguez-Prieto [1,3], Ana María Aragón [1,3], Cinta Lorenzo-Martín[3], Ángel Yanguas-Gil [3]

[1] Department of Manufacturing Engineering, Universidad Nacional de Educación a Distancia (UNED), Madrid, Spain; jprado28@alumno.uned.es; amcamacho@ind.uned.es; alvaro.rodriguez@invi.uned.es; amaragon@invi.uned.es

2 Department of Design in Engineering, University of Vigo, C/ Torrecedeira 86, 36208, Vigo (Pontevedra), Spain, jdieguez@uvigo.es

3 Applied Materials Division, Argonne National Laboratory, 9700 Cass Ave, Lemont, IL 60439, USA., prodriguez@anl.gov; aargn@anl.gov; lorenzo-martin@anl.gov; ayg@anl.gov

* Correspondence: amcamacho@ind.uned.es; Tel.: +34-913-988-660

Received: date; Accepted: date; Published: date

Abstract: One of the challenges in Additive Manufacturing (AM) of metallic materials is to obtain workpieces free of defects with excellent physical, mechanical and metallurgical properties. In Wire and Arc Additive Manufacturing (WAAM) the influences of process conditions on thermal history, microstructure and resultant mechanical and surface properties of parts need to be deeply analyzed. In this work, 3D metallic parts of mild steel wire (AWS ER70S-6) are built with a WAAM process by depositing layers of material on a substrate of a S235 JR steel sheet of 3 mm thickness under different process conditions, using as welding process Gas Metal Arc Welding (GMAW) with Cold Metal Transfer technology, combined with a positioning system as a CNC milling machine. Considering the hardness profiles, the estimated Ultimate Tensile Strengths (UTS) derived from hardness measurements and the microstructure findings, it can be concluded that the most favourable process conditions are the ones provided by CMT, with homogeneous hardness profiles, good mechanical strengths in accordance to conditions defined by standard, and without formation of a decohesionated external layer; being the CMT Continuous the optimal option as the mechanical properties are slighter better than with single CMT.

Keywords: Additive manufacturing; WAAM; GMAW; Cold Metal Transfer; Hardness; Mechanical properties; Thermal input; Microstructure

1. Introduction

One of the challenges in Additive Manufacturing (AM) of metallic materials is to obtain workpieces free of defects and with excellent physical, mechanical and metallurgical properties [1] to satisfy the strict requirements of engineering applications. Obtaining such mechanical requirements is a hard task especially in parts fabricated as the result of layer by layer addition of the material. AM of metallic materials involves different techniques (powder bed fusion, binder jetting, sheet lamination and directed energy deposition) and metals generally must be weldable and castable to be successfully processed in AM [2]. Most of the current commercial metallic materials for AM are steels [3–6], aluminum [7] and titanium alloys [8,9].

Wire and Arc Additive Manufacturing (WAAM) is a wire-feed AM process and one of the most promising techniques for producing larger components with moderate complexity and relative low costs compared to other AM techniques for metals [10]. WAAM processes generally involve high residual stresses due to high deposition rates and heat inputs [11]. The influences of process conditions (for example, energy input, wire-feed rate [12], welding speed and/or deposition pattern [13]) on thermal history, microstructure and resultant mechanical and surface properties of parts need to be deeply analyzed [11] as there is not enough knowledge in the scientific community yet.

As explained in the work by Ge et al. [4], during WAAM processes, the added layers of material suffer a complicated thermal history that includes, among others, melting, fast cooling, solidification, and/or partial remelting, that greatly influence the final properties of the parts produced by these techniques.

A recent study about the microstructure is the one from Wang et al. [14], where mechanical properties of thin-walled parts of the die steel H13 were also analysed, showing that the tensile properties were anisotropic but could become isotropic after 830 °C of heat treatment (annealing) for 4 hours. Yan et al. [15] studied the effect of temperature gradient, solidification velocity and alloy composition on grain morphology in AM of metallic materials. In the overview article of Herzog et al. [16], special attention was paid in analysing AM specific grain structures, resulting from the complex thermal cycle and high cooling rates. Kok et al. [17] reviewed the anisotropy and heterogeneity of microstructure and mechanical properties of metallic parts manufactured by AM, highlighting that the main factors influencing these two characteristics were either their microstructural features and manufacturing deficiencies. On the other hand, in the work from Szost et al. [18], porosity, microstructure and micro hardness of Al-6.3%Cu samples fabricated by WAAM were investigated considering cold metal transfer (CMT) variants, pulsed CMT and advanced CMT.

Mechanical properties obtained by WAAM, including hardness, are also a promising field of study as shown in works from Horgar et al. [19], where AA5183 aluminium alloy wire was deposited on AA6082-T6 plate as substrate. Wu et al. [20] investigated the influence of the molten pool size on microstructure and mechanical properties of pieces of Ti-6Al-4V alloy, whereas Lewandowski and Seifi [21] presented a review of mechanical properties for the most common alloys used in AM of metals (Ti-6Al-4V, TiAl, stainless steel, Inconel 625/718, and Al-Si-10Mg).

Micro-geometrical properties such as roughness are also being investigated, as in the case of manufacturing of multi-layer single-pass thin-walled parts [22] and in the work of Li et al. [23].

Till now, there have been only a limited number of commercial alloys used in AM [24], so there is a need to increase the number of alloys to be processes by AM techniques in order to widen the application fields.

In this work, 3D metallic parts of mild steel wire (AWS ER70S-6) are built with a WAAM process by depositing beads of weld metal layer by layer on a substrate of a S235 JR steel sheet of 3 mm thickness, using as welding process Gas Metal Arc Welding (GMAW) [25] with Cold Metal Transfer technology [26], combined with a positioning system as a CNC milling machine [27]. The paper will show some interesting results based on measurements on hardness, along with complementary values of tensile strength at the working area and microstructure information.

2. Materials and Methods

2.1. Materials for WAAM process

Experiments have been carried out on a substrate of a S235 JR steel sheet of 3 mm thickness, 150 mm long and 100 mm wide. This substrate has two main functions: as a support for the deposited metal and as a heat dissipation system for the heat generated during the process by conduction transfer through the aluminum work table.

The wire material (AWS ER70S-6) is a 0.8 mm diameter mild steel wire with a copper coating supplied on a 15 kg coil. This steel is commonly used in a lot of applications related to construction works, pipes, shafts, car bodies, tanks, steel castings or forgings and general shop fabrications.

The properties of the base material (substrate) and the deposited material are shown in Table 1. The density of both materials is approximately the same, while the mechanical properties are better for the case of the deposited material.

Table 1. Properties of the substrate and the welding wire

Mechanical properties	S235 JR	AWS ER70S-6
Density (kg/m³)	7800	7833
Yield point (MPa)	235	420
UTS (MPa)	370-510	500-640

Chemical composition of welding wire is shown in the Table 2.

Table 2. Chemical composition of welding wire

Element	C	Mn	S	Ni	V	Cr	Cu	Si	P	Mo
wt%	0.06-0.15	1.40-1.85	0.035 max	0.15 max	0.03 max	0.15	0.50	0.80-1.15	0.025	0.15 max

The results of the process depend on the protecting gas. It has been used a mixture composed of CO_2 (15%) and Argon (85%) that led to stability of the process, improvement in the surface finishing quality and reduction of the splatters. It has been observed that the welding drops are smaller with the reduction of the amount of CO_2.

2.2. WAAM Equipment

The WAAM equipment is composed by two different systems (Figure 1), as described in detail in a previous work [28]:

- Welding system. Cold Metal Transfer technology, patented by Fronius®, was used as welding process with a Fronius TPS 4000 CMT R machine. In this technology the intensity and voltage control is made during the deposition. By virtue of this principle, the temperature of welding temperature is reduced and the wire movement is optimized. As a result of this, the quality of weld beads is better than using conventional GMAW welding [29].
- Positioning system. The control of the movement in an easy way was made by a BF 30 Vario Optimum CNC milling machine. It has been adapted fixing the welding torch to the milling head in the Z axis, while the X-Y table of the CNC system enables the deposition of a layer in the fixed Z level. To deposit the next layer, the Z axis elevates the torch and makes the deposition in the next Z level.

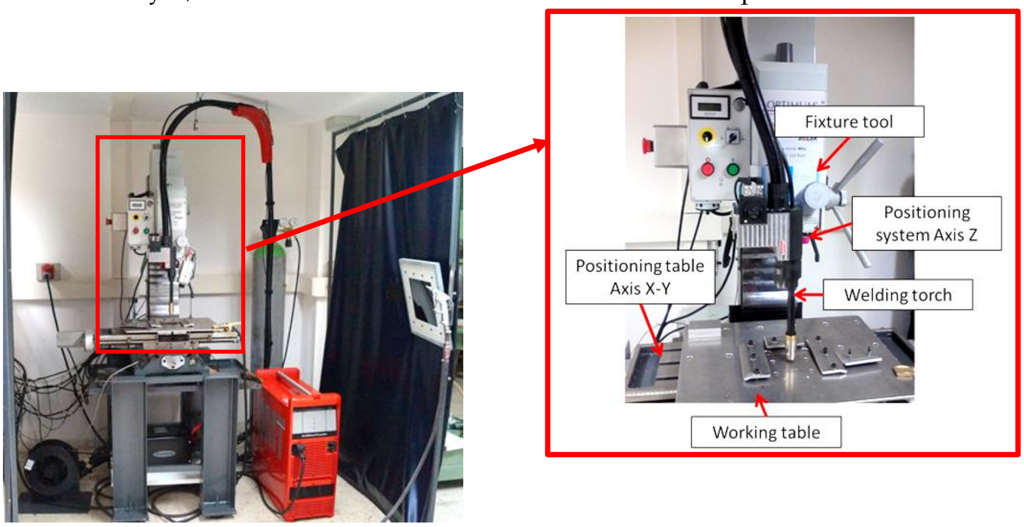

Figure 1. Setup of the integrated WAAM system in the positioning table

As shown in Figure 1, an auxiliary working table has been developed in order to isolate electrically both systems as well as to cool the working area.

2.3. Fabrication of samples by WAAM

As explained in a previous work [28], in WAAM processes, the final product is manufactured by melting a wire using an electric arc (Figure 2). The deposition of the material rate is much higher with respect to other metallic additive manufacturing methods. In addition, higher working speeds allow higher workload and a significantly lower price than with other methods [30].

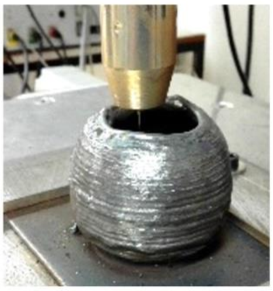

Figure 2. Examples of geometries obtained by WAAM.

In this work, a set of WAAM samples have been manufactured under different process conditions, considering the parameters with more influence in the mechanical properties of WAAM parts:

- WAAM process (MIG, CMT, CMT Advance pol -5, CMT Advance pol 0, CMT Advance pol 5, CMT continuous trajectory)
- Welding speed (constant = 400 mm/min)
- Deposition speed (constant = 2.5 m/min)
- Arc voltage (constant = 9.2 V)
- Current intensity (50 A, 66 A, 70 A, 78 A)
- Layer step (1.0 mm, 1.5 mm)

Different WAAM processes have been also applied to analyze the influence of using a conventional MIG process, a MIG process with CMT, and a MIG process with CMT advanced and different current polarities.

Cold Metal Transfer welding (CMT) is based on MIG welding process but modified by a short-circuiting transfer process, firstly developed by Fronius Austria in 2004 [26]. CMT provides controlled method of material deposition and low thermal input by incorporating an innovative wire feed system coupled with high-speed digital control [31]. With CMT the arc only introduces any heat for a very brief period during the arc-burning phase; the arc remains stable and then CMT can be used everywhere and in every position [32].

The CMT advanced is an evolution of the previous process and it allows to obtain a lower thermal input during welding with respect to the original CMT process thanks to the possibility of polarity change. This produces the reversal of the direction of the plasma jet several times per second leading to a 35-40% lower thermal inputs [33]. The reversal of polarity takes place in the short-circuit phase so that this welding process guarantees the high stability expected from cold welding [34]. Thermal input is usually calculated based on the Eq.1:

$$TI = \frac{V \cdot I \cdot \mu}{welding\ speed} \tag{1}$$

Where TI is the thermal input in J/mm, V is the arc voltage in volts (V), I is the process intensity in Amperes (A), μ is the thermal efficiency that is a constant coefficient based upon the welding process used; finally, the welding speed is provided in mm/s.

The samples and the definition of parameters used are presented in Table 3, including the calculation of thermal input.

Table 3. Definition of parameters used for each sample and results.

Nº	Process	Intensity (A)	Thermal input*[1] (J/mm)	Welding Speed (mm/min)	Deposition Speed (m/min)	Wall thickness (mm)	Layer step (mm)	Total height (mm)	Layer height (mm)
1	MIG	50	55.19	400	2.5	3.8	1.0	27.0	0.90
2	CMT	50	35.87	400	2.5	3.7	1.0	30.7	1.02
3	CMT Adv pol 0	70	50.22	400	2.5	4.2	1.0	20.2	1.44
4	CMT Adv pol 0	70	50.22	400	2.5	5.5	1.5	35.5	0.92
5	CMT Adv pol -5	66	47.36	400	2.5	4.5	1.5	41.2	1.07
6	CMT Adv pol +5	78	55.97	400	2.5	6.6	1.5	33.4	0.80
7	CMT Cont.	50	35.87	400	2.5	3.1	1.0	30.5	1.02

[1] Note 1*: thermal input has been calculated based on the power (*V·I*) provided by the equipment, the welding speed and the thermal efficiency coefficients, typically μ (MIG)= 0.8, and μ (CMT)=0.52 considering a 35% of lower thermal efficiency compared to MIG process [33].

Samples nº 2 and 7 share the same WAAM parameters; however, sample nº 7 differs from sample nº 2 in the way the wire is deposited. In order to provide a continuity during the deposition process, and to avoid edge effects, sample nº 7 has been obtained using a continuous tool path as shown in Figure 3b (CMT Continuous trajectory). Afterwards, the sample has been cut; the final samples obtained are shown in Figure 3c.

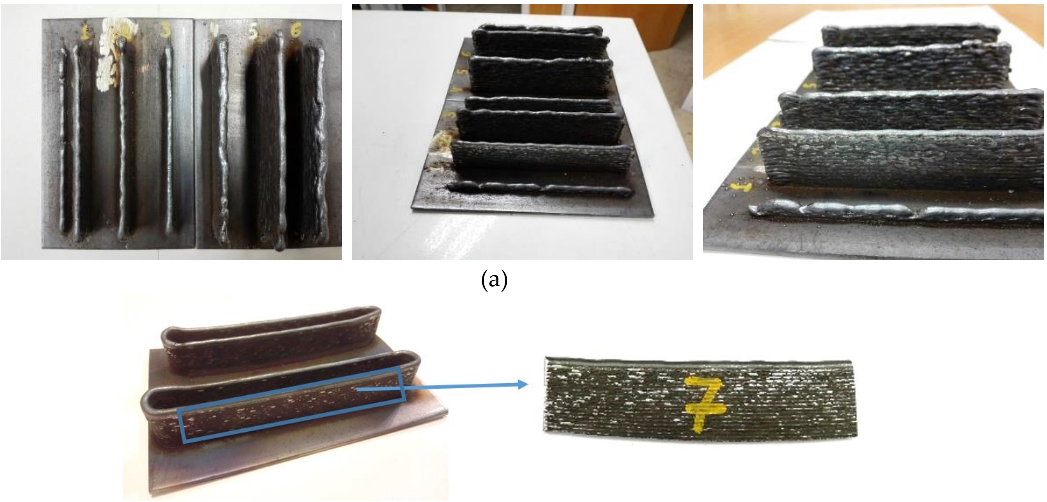

(a)

(b)

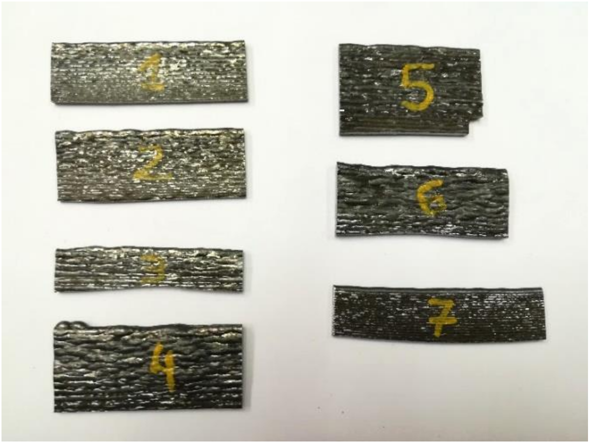

(c)

Figure 3. (**a**) Manufacturing of samples nº 1 to 6; (**b**) Configuration of tool path during the deposition process in sample nº 7; **(c)** Final 7 WAAM Samples.

2.4. Brinell hardness tests

2.4.1. Brinell hardness tests and measurement of the ball prints

Brinell hardness tests have been developed [35] using a ball indenter of ϕ2.5 mm and a test force of 612.9 N (Figure 4).

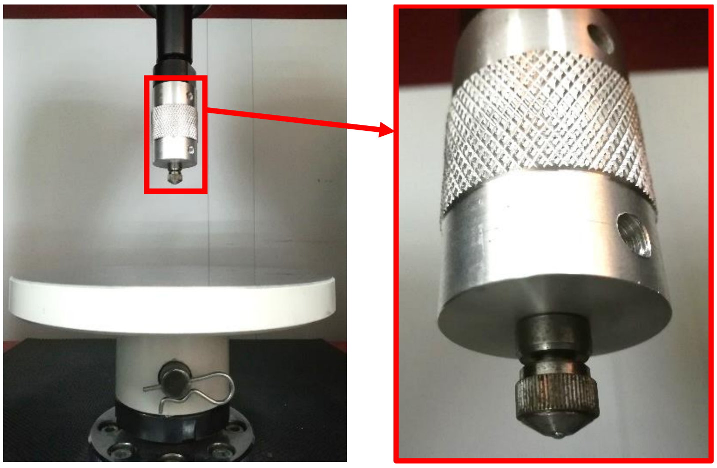

Figure 4. Brinell hardness tests setup and detail of the ball indenter.

The ball prints imprinted at the surface of the 7 samples are presented in Figure 5. A set of 5 points have been imprinted at the surfaces, that have been previously polished to obtain a smooth condition and free from oxides and lubricants. The numbering of the points is increasing from the location of the substrate. The aim is to obtain a hardness profile for each sample in order to compare the observed behaviour depending on the manufacturing parameters used in each case.

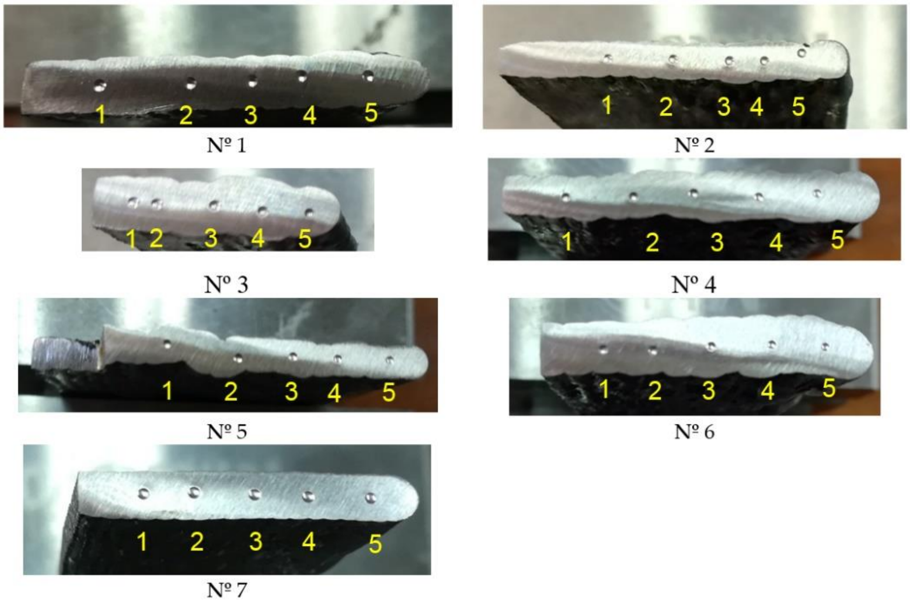

Figure 5. Brinell hardness tests applied to WAAM samples and identification of indentation points.

The measurement device to determine experimentally the print diameter is a profile projector TESA VISIO (Figure 6). Two indentation diameters measured at 90° have been obtained for each sample allowing to calculate a mean diameter of the indentation.

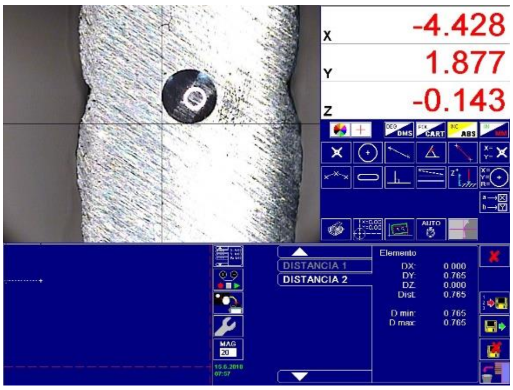

Figure 6. Example of measurement of ball print diameter of WAAM samples with Profile projector TESA VISIO.

The Brinell hardness is proportional to the quotient obtained by dividing the test force by the surface area of the indentation left in the surface after removal of the test force.

The dispersion among measurements can be quantified using the reproducibility limit, *R*, which is calculated as shown in Eq.2 [36]:

$$R = \frac{d_{max} - d_{min}}{< d >} \tag{2}$$

Where d_{max} and d_{min} are the largest and smallest diameters and $<d>$ is the mean of measured diameters.

2.5. Determination of mechanical strength

Hardness is usually defined as resistance to permanent indentation. This testing provides a measurement of the material strength through its resistance to scratching. Thus, the possibility to predict tensile strength based on values of materials hardness is often used. Eq. 3 provides the general relationship between hardness and tensile strength:

$$UTS = k \cdot H \quad (3)$$

Where UTS is the ultimate tensile strength in MPa, H the hardness in a known scale and k is a coefficient. Several standards provide a correlation between hardness and tensile strength in steels using tables, charts and coefficients of calculation, some of them are ASTM A370 [37], ISO 18265 [36], SAE J417 [38], being the ASTM standard the most consolidated and used.

2.5. Equipment and measurement of microstructure

Microstructural analysis has been performed using the following equipment of Center for Nanoscale Materials (CNM) of Argonne National Laboratory: a high resolution and high vacuum, scanning electronic microscopy Hitachi S-4700-II —equipped with EDS detector Bruker XFlash 6160. The testing conditions were 10 keV and 10 mA.

3. Results

3.1. Evaluation of hardness profiles

Before analyzing the hardness profiles, it is important to show the position of the indentations of every point imprinted at the surface. As the WAAM process is layer-based, we want to check if there is any influence of the position when indentation points are located at the overlapping area of two layers, compared to those ones close to the middle of a single layer. In Figure 7 the position of the points for every sample is shown.

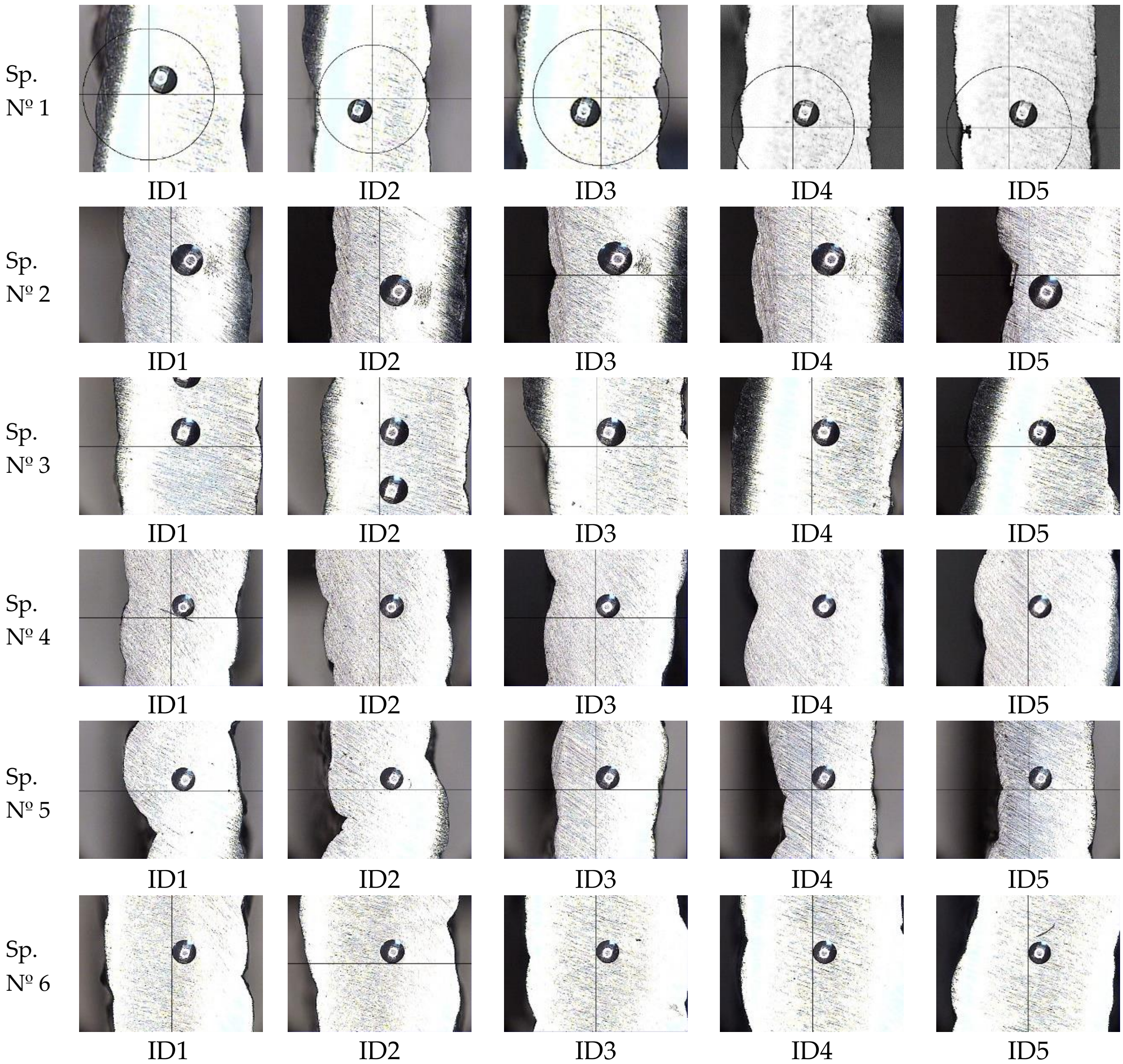

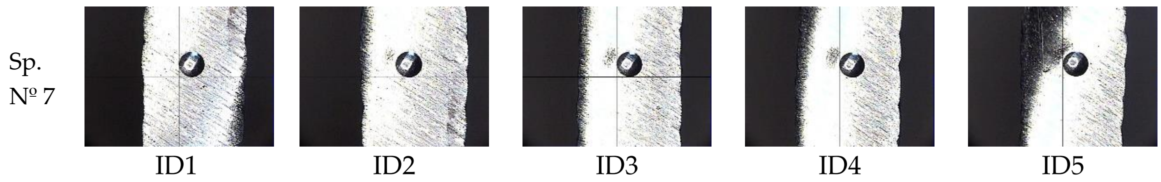

Figure 7. Brinell hardness tests applied to WAAM samples and identification of indentation points.

Table 4 provides the mean values of Brinell hardness along with the thermal input and the calculation of reproducibility limit (*R*) according to Eq.2, using the diameters of indentations.

Table 4. Process, Brinell hardness and *R* values

Sample nº	Process	Thermal input (J/mm)	Brinell hardness (mean value)	<*d*>	d_{max}	d_{min}	*R*
1	MIG	55.19	172.89	0.729	0.731	0.7285	0.003
2	CMT	35.87	142.14	0.790	0.809	0.759	0.064
3	CMT Adv pol 0	50.22	159.03	0.761	0.790	0.725	0.086
4	CMT Adv pol 0	50.22	153.00	0.778	0.799	0.759	0.051
5	CMT Adv pol -5	47.36	154.49	0.773	0.789	0.759	0.038
6	CMT Adv pol +5	55.97	148.84	0.792	0.815	0.771	0.056
7	CMT Cont.	35.87	152.67	0.772	0.784	0.765	0.025

Conventional MIG (sample 1) process provides the biggest thermal input and hardness along with the minimum *R* value (0.003). CMT process (samples 2 and 7), with the lowest thermal inputs, provides and adequate dispersion among values, exhibited by their R values (0.064 and 0.025, respectively). Hardness values in samples 3 to 6 (CMT advanced) do not seem to follow a pattern dependent to thermal input, but hardness and thermal inputs adopt intermediate values.

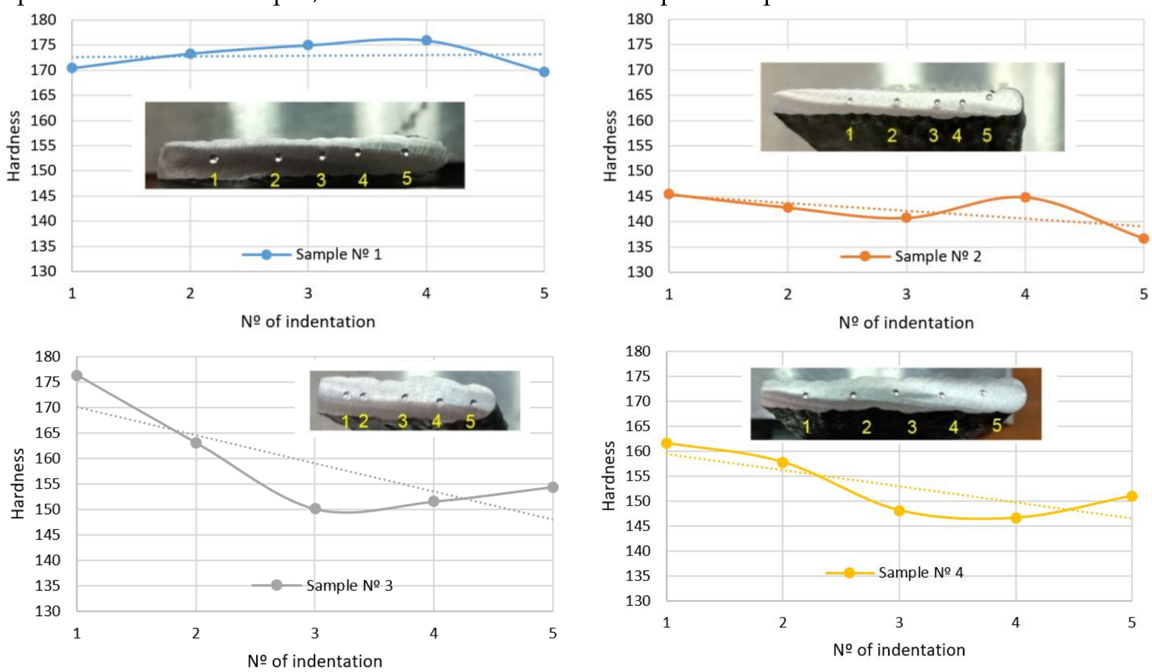

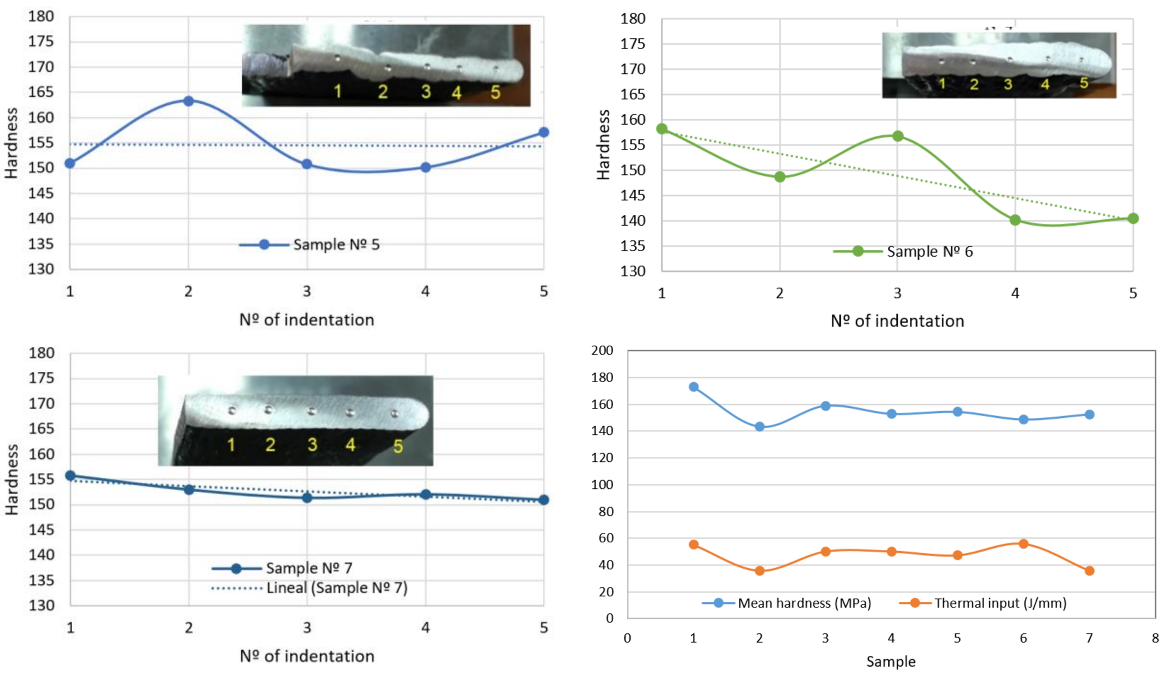

Figure 8. Brinell hardness profiles for the WAAM samples, mean hardness values and thermal inputs.

The hardness profiles are presented in Figure 8 along with the average values. A homogenous hardness profile is desirable as this means that the mechanical properties obtained by the WAAM process are appropriate and the in-service behaviour of parts is expected to be better than with non-homogeneous ones.

3.2. Evaluation of mechanical strength

Using the hardness measurements, estimated Ultimate Tensile Strengths (UTS) have been calculated as provided in Table 5.

Table 5. Estimation of Ultimate Tensile Strength values based on ASTM A370 [37]

		Process						
	ID	**MIG**	**CMT**	**CMT Adv p. 0**	**CMT Adv p. 0**	**CMT Adv p.-5**	**CMT Adv p. +5**	**CMT-Cont.**
UTS (MPa) correlation per indentation according to Fig.8.	**1**	573.33	479.99	516.38	498.34	498.39	467.42	528.44
	2	583.30	473.06	499.98	483.64	562.20	465.82	505.24
	3	587.47	468.90	495.17	488.64	497.70	534.68	499.66
	4	589.84	477.92	561.66	541.73	495.74	490.68	501.99
	5	572.46	454.32	590.94	558.59	537.12	544.38	498.00
Mean		581.28	470.84	532.82	514.19	518.23	500.59	506.67

As it was previously mentioned, the welding wire is ER70S-6 type, described by ASME SFA 5.18 standard [39], which indicates some recommended base materials to be welded using this type of welding wire; these are SA-36 [40], equivalent to S235JR, SA-285 [41], SA-515 [42] and SA-516 [43]. Table 6 exhibits the specified range of UTS for these materials. These values are used to help analyze the ultimate tensile strength (UTS) calculated using the hardness measurement performed in the 7 samples.

Table 6. Ultimate Tensile Strength of typical base materials welded with ER70S-6 according to SFA 5.18 [39]

Base material specification	UTS (MPa)
SA-36 (equivalent to S235JR)	400-550
SA-285	310-515
SA-515	415-485
SA-516	380-485

3.3. Evaluation of microstructure

Microstructural analysis of each sample (1 to 7) has been performed using a high-resolution scanning electronic microscopy at the Center for Nanoscale Materials (CNM) of Argonne National Laboratory. Figure 9 shows the surface of deposited material along the thickness according the disposition indicated in Figure 3c.

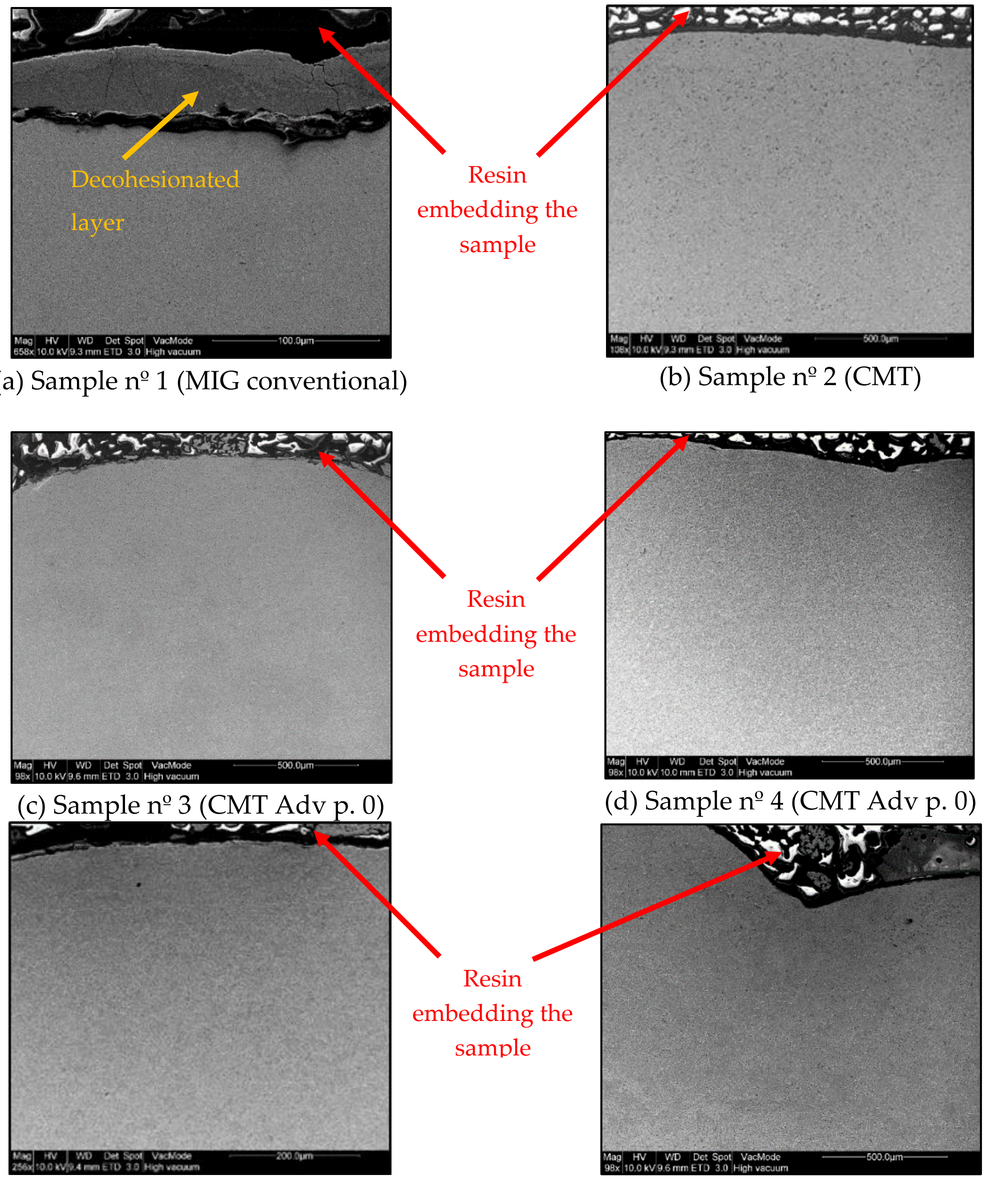

(a) Sample nº 1 (MIG conventional) (b) Sample nº 2 (CMT)

(c) Sample nº 3 (CMT Adv p. 0) (d) Sample nº 4 (CMT Adv p. 0)

(e) Sample nº 5 (CMT Adv p. -5) (f) Sample nº6 (CMT Adv p. +5)

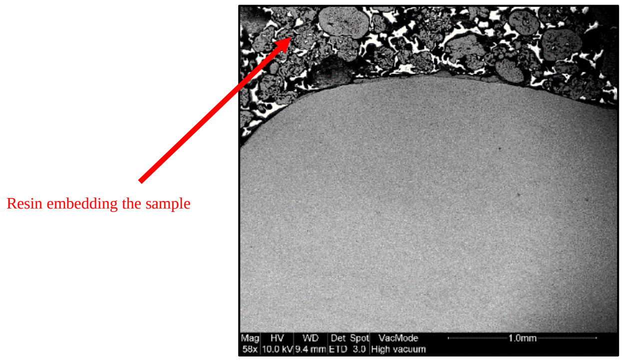

(g) Sample nº 7 (CMT)

Figure 9. Scanning electronic microscopy (SEM) performed to observe the transition between melted layers. a) Sample nº 1, MIG (conventional), b) Sample nº 2, CMT process, c) Sample nº 3, CMT Adv p.0, d) Sample nº 4, CMT Adv p.0, e) Sample nº5, CMT Adv p.-5, f) Sample nº 6, CMT Adv p.+5, g) Sample nº 7, CMT.

Figure 9 provides images of the surface along the deposition direction. In Figures 9a to 9g, homogeneity can be observed in the transition between layers. Nevertheless, a decohesionated layer in the upper edge is observed in Figure 9a (MIG conventional). Figure 10 shows the microstructure of this layer at 20 μm.

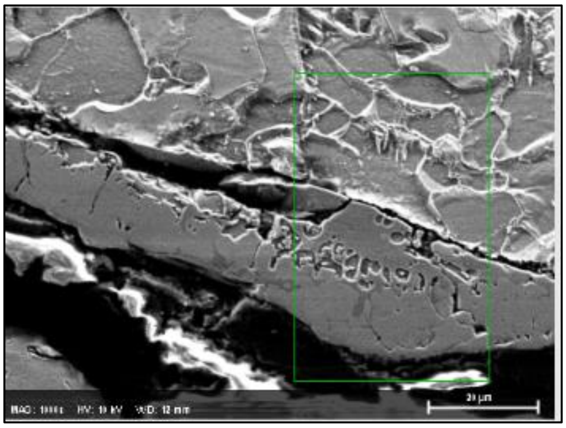

Figure 10. Layer SEM image at 20 μm of scale

Table 7 provides the compositional microanalysis of this layer observed in sample nº 1.

Table 7. Microanalysis of decohesionated external layer observed in Sample 1 (MIG conventional process)

Element	Mn	C	O	Si	Cu	Fe
wt%	1.58	7.59	1.79	0.83	0.44	87.77

The external layer of sample 1 (MIG process) seems to be formed by Fe_3C (6.67%C) and probably other complex carbides made up of some of the rest elements oxidized but present in normal weight percentage according to the composition provided by the manufacturer (Mn 1.40-1.85%, Si 0.80-1.15%, Cu<0.5%). In addition, in the process magnetite (Fe_3O_4) seems to be also present. Anyway, the external layer is pernicious effect that could be avoid using CMT process, as it is possible to see through Figures 9b to 9g.

4. Discussion

As indicated, a homogenous hardness profile is desirable as this means that the mechanical properties obtained by the WAAM process lead to better in-service behaviour of parts than with non-homogeneous ones.

The most homogeneous profiles are obtained in samples numbers 1, 2 and 7 (in sample 2 the measurement of point 5 has been obviated as the print is too close to the surface). Homogeneous profiles for MIG procedure (sample 1) were also obtained in the work by Wang et al. [14]. Samples 2 and 7 present lower values of hardness than sample 1 (Table 4); this can be explained as the CMT process applies lower thermal inputs compared to the conventional MIG process and therefore, the sample 1 experience greater sub-cooling from the melting state and then, a microstructure of finer grains is expected. Bigger grain sizes at the microstructure lead to lower hardness values as grains limits contribute to block the movement of material dislocations.

Slight differences between sample 2 (CMT) and 7 (CMT Cont) are due to the effect of the continuous path applied in sample 7 that, for the same thermal input due to the same process parameters, implies an accumulation of heat at the zone due to the lower heat transmission and consequently, induces a higher thermal input than the one computed and, as explained before, this leads to a higher hardness value in sample 7.

Samples fabricated by CMT Advanced processes have a pronounced decreasing trend of the hardness profile, showing the highest values closer to the substrate. This is due to the chilling effect of the substrate that generates a higher cooling rate and therefore, the sub-cooling effect from the melting state is higher in this zone [4]. The results are in good agreement with the ones presented by Liberini et al. in their work from 2017 [44]; where an increase of hardness is also found close to the free surface as a result of the thermal chilling due to the contact with the air at room temperature. In this work [44], the authors also stated that the cooling curve is the factor that most influences the final microstructure and that no important differences between the samples are obtained from different process parameters. With CMT Advanced, the mean hardness values are very similar for samples 3 to 6, and the thermal inputs as well.

The most inhomogeneous profiles are obtained in samples 5 and 6, where some peaks are observed. In these two cases a polarity of 5 and +5, respectively, is applied during the process, and the intensity applied is also different in both cases (66 and 78 A, respectively). However, regardless the different conditions, the mean hardness values are close between them and to the ones obtained with polarity 0. In general, we can conclude that the CMT Advanced process is not showing a better performance of the process regarding the homogeneity of the hardness profile of the parts and so the mechanical properties.

No significant influence of the position of indentation points on the hardness values is observed, when indentation points are located at the overlapping area of two layers, compared to those ones close to the middle of a single layer.

As WAAM is a layer-by-layer manufacturing process by using a welding wire that melts on a previously welded substrate, it is important to ensure that the requirements of weldability, such as the mechanical properties of material that is joined using the welding wire, are well suited. Using the recommendations provided by the Kobe Welding Handbook [45], the base material should present a minimum UTS between 400-480 MPa. Therefore, considering the requirements indicated in Table 6, in this evaluation, a range between 400 and 550 is considered suitable. Values higher than 550 MPa could lead to the appearance of hardness peaks between layers, which are not recommended as they do not guarantee the homogeneity of the mechanical behaviour. This supposes that the estimated UTS at the surface of sample 1 (MIG conventional process), equal to 581.28 MPa, is greater than the upper limit that the new substrate should exhibit. The remaining mean values (samples 2 to 7) are between 400 and 550 MPa, nevertheless some specific values are above the upper limit (550 MPa) in samples 3 to 5. Thus, it can be concluded that CMT process (samples 2 and 7) and CMT advance pol.+5 (sample 6) provides the most adequate UTS values.

In addition, microstructural analysis of each sample (1 to 7) has been performed using a high-resolution scanning electronic microscopy. Homogeneity has been observed in the transition between layers in all samples. Nevertheless, a decohesionated layer in the upper edge is observed in sample 1 (MIG conventional). The external layer is a pernicious effect that can be avoid using CMT process.

In agreement with other authors, there are no significant differences between the samples processed with different process parameters when using a particular WAAM process [11,44].

After this analysis, considering the hardness profiles, the estimated Ultimate Tensile Strengths (UTS) derived from hardness measurements and the microstructure findings, it can be concluded that the best process conditions are the ones provided by CMT, with homogeneous hardness profiles, good mechanical strengths in accordance to conditions defined by standard, and without formation of a decohesionated external layer; being the CMT Continuous the optimal option as the mechanical properties are slighter better than with single CMT.

Author Contributions: Conceptualization, José Luis Prado-Cerqueira, Ana María Camacho, José Luis Diéguez and Álvaro Rodríguez-Prieto; Formal analysis, José Luis Prado-Cerqueira, Álvaro Rodríguez-Prieto, Ana María Aragón and Cinta Lorenzo; Funding acquisition, José Luis Prado-Cerqueira, Ana María Camacho, José Luis Diéguez and Ángel Yangüas-Gil; Investigation, José Luis Prado-Cerqueira, Ana María Camacho, José Luis Diéguez, Álvaro Rodríguez-Prieto, Ana María Aragón and Cinta Lorenzo; Methodology, José Luis Prado-Cerqueira, Ana María Camacho and Álvaro Rodríguez-Prieto; Project administration, Ana María Camacho; Resources, José Luis Prado-Cerqueira, José Luis Diéguez and Ángel Yangüas-Gil; Supervision, Ana María Camacho; Validation, José Luis Prado-Cerqueira; Writing – original draft, José Luis Prado-Cerqueira; Writing – review & editing, Ana María Camacho, José Luis Diéguez, Álvaro Rodríguez-Prieto and Ángel Yangüas-Gil.

Funding: This research was funded by the program "Innova" of the Galician Department of Education (Spain) and the APC was funded by the Annual Grants Call of the E.T.S.I.I. of UNED through the project of reference [2018-ICF04]. A mobility grant for junior researchers has been also granted by MES (Manufacturing Engineering Society) to Álvaro Rodríguez-Prieto.

Acknowledgments: This work has been developed within the framework of the doctorate program in Industrial Technologies of the UNED and in the context of the project DPI2016-81943-REDT of the Ministry of Economy, Industry and Competitiveness and the LDRD Project "Metal additive manufacturing modeling" with reference 2017-042-N0 of Argonne National Laboratory. We would like to extend our acknowledgement to the Department of Mechanical Manufacturing of the I.E.S. Politécnico de Vigo and the Manufacturing Engineering Department of the University of Vigo. The authors also acknowledge the Research Group of the UNED "Industrial Production and Manufacturing Engineering (IPME)", Carlos Romano and Carlos Vicente for the given support during the development of this work and the Applied Materials Division of Argonne National Laboratory. We also acknowledge to Center for Nanoscale Materials (CNM), supported by the US Department of Energy, Office of Science and Office of Basic Energy Sciences under Contract Nº. DE-AC02-06CH11357.

Conflicts of Interest: The authors declare no conflict of interest. The funders had no role in the design of the study; in the collection, analyses, or interpretation of data; in the writing of the manuscript, and in the decision to publish the results.

References

1. Singh, S.; Ramakrishna, S.; Singh, R. Material issues in additive manufacturing: A review. *J. Manuf. Process.* **2017**, *25*, 185–200, doi:10.1016/J.JMAPRO.2016.11.006.
2. Bourell, D.; Kruth, J. P.; Leu, M.; Levy, G.; Rosen, D.; Beese, A. M.; Clare, A. Materials for additive manufacturing. *CIRP Ann.* **2017**, *66*, 659–681, doi:10.1016/J.CIRP.2017.05.009.
3. Xu, X.; Ganguly, S.; Ding, J.; Guo, S.; Williams, S.; Martina, F. Microstructural evolution and mechanical properties of maraging steel produced by wire + arc additive manufacture process. *Mater. Charact.* **2017**, doi:10.1016/J.MATCHAR.2017.12.002.
4. Ge, J.; Lin, J.; Lei, Y.; Fu, H. Location-related thermal history, microstructure, and mechanical properties of arc additively manufactured 2Cr13 steel using cold metal transfer welding. *Mater. Sci. Eng. A* **2018**, *715*, 144–153, doi:10.1016/J.MSEA.2017.12.076.
5. Hu, Z.; Qin, X.; Shao, T. Welding Thermal Simulation and Metallurgical Characteristics Analysis in WAAM for 5CrNiMo Hot Forging Die Remanufacturing. *Procedia Eng.* **2017**, *207*, 2203–2208,

doi:10.1016/J.PROENG.2017.10.982.

6. Artaza, T.; Alberdi, A.; Murua, M.; Gorrotxategi, J.; Frías, J.; Puertas, G.; Melchor, M. A.; Mugica, D.; Suárez, A. Design and integration of WAAM technology and in situ monitoring system in a gantry machine. *Procedia Manuf.* **2017**, *13*, 778–785, doi:10.1016/J.PROMFG.2017.09.184.
7. Luo, Y.; Li, J.; Xu, J.; Zhu, L.; Han, J.; Zhang, C. Influence of pulsed arc on the metal droplet deposited by projected transfer mode in wire-arc additive manufacturing. *J. Mater. Process. Technol.* **2018**, *259*, 353–360, doi:10.1016/J.JMATPROTEC.2018.04.047.
8. Wu, B.; Pan, Z.; Li, S.; Cuiuri, D.; Ding, D.; Li, H. The anisotropic corrosion behaviour of wire arc additive manufactured Ti-6Al-4V alloy in 3.5% NaCl solution. *Corros. Sci.* **2018**, *137*, 176–183, doi:10.1016/J.CORSCI.2018.03.047.
9. Shi, X.; Ma, S.; Liu, C.; Wu, Q.; Lu, J.; Liu, Y.; Shi, W. Selective laser melting-wire arc additive manufacturing hybrid fabrication of Ti-6Al-4V alloy: Microstructure and mechanical properties. *Mater. Sci. Eng. A* **2017**, *684*, 196–204, doi:10.1016/J.MSEA.2016.12.065.
10. Cunningham, C. R.; Wikshåland, S.; Xu, F.; Kemakolam, N.; Shokrani, A.; Dhokia, V.; Newman, S. T. Cost Modelling and Sensitivity Analysis of Wire and Arc Additive Manufacturing. *Procedia Manuf.* **2017**, *11*, 650–657, doi:10.1016/J.PROMFG.2017.07.163.
11. Ding, D.; Pan, Z.; Cuiuri, D.; Li, H. Wire-feed additive manufacturing of metal components: technologies, developments and future interests. *Int. J. Adv. Manuf. Technol.* **2015**, *81*, 465–481, doi:10.1007/s00170-015-7077-3.
12. Geng, H.; Li, J.; Xiong, J.; Lin, X.; Zhang, F. Optimization of wire feed for GTAW based additive manufacturing. *J. Mater. Process. Technol.* **2017**, *243*, 40–47, doi:10.1016/j.jmatprotec.2016.11.027.
13. Venturini, G.; Montevecchi, F.; Scippa, A.; Campatelli, G. Optimization of WAAM Deposition Patterns for T-crossing Features. *Procedia CIRP* **2016**, *55*, 95–100, doi:10.1016/J.PROCIR.2016.08.043.
14. Wang, T.; Zhang, Y.; Wu, Z.; Shi, C. Microstructure and properties of die steel fabricated by WAAM using H13 wire. *Vacuum* **2018**, *149*, 185–189, doi:10.1016/J.VACUUM.2017.12.034.
15. Yan, F.; Xiong, W.; Faierson, E. Grain Structure Control of Additively Manufactured Metallic Materials. *Materials (Basel).* **2017**, *10*, 1260, doi:10.3390/ma10111260.
16. Herzog, D.; Seyda, V.; Wycisk, E.; Emmelmann, C. Additive manufacturing of metals. *Acta Mater.* **2016**, *117*, 371–392, doi:10.1016/j.actamat.2016.07.019.
17. Kok, Y.; Tan, X. P.; Wang, P.; Nai, M. L. S.; Loh, N. H.; Liu, E.; Tor, S. B. Anisotropy and heterogeneity of microstructure and mechanical properties in metal additive manufacturing: A critical review. *Mater. Des.* **2018**, *139*, 565–586, doi:10.1016/j.matdes.2017.11.021.
18. Szost, B. A.; Terzi, S.; Martina, F.; Boisselier, D.; Prytuliak, A.; Pirling, T.; Hofmann, M.; Jarvis, D. J. A comparative study of additive manufacturing techniques: Residual stress and microstructural analysis of CLAD and WAAM printed Ti–6Al–4V components. *Mater. Des.* **2016**, *89*, 559–567, doi:10.1016/J.MATDES.2015.09.115.
19. Horgar, A.; Fostervoll, H.; Nyhus, B.; Ren, X.; Eriksson, M.; Akselsen, O. M. Additive manufacturing using WAAM with AA5183 wire. *J. Mater. Process. Technol.* **2018**, *259*, 68–74, doi:10.1016/J.JMATPROTEC.2018.04.014.
20. Wu, Q.; Lu, J.; Liu, C.; Fan, H.; Shi, X.; Fu, J.; Ma, S. Effect of molten pool size on microstructure and tensile properties of wire arc additive manufacturing of Ti-6Al-4V alloy. *Materials (Basel).* **2017**, doi:10.3390/ma10070749.
21. Lewandowski, J. J.; Seifi, M. Metal Additive Manufacturing: A Review of Mechanical Properties. *Annu.*

Rev. Mater. Res. **2016**, *46*, doi:10.1146/annurev-matsci-070115-032024.
22. Xiong, J.; Li, Y.; Li, R.; Yin, Z. Influences of process parameters on surface roughness of multi-layer single-pass thin-walled parts in GMAW-based additive manufacturing. *J. Mater. Process. Technol.* **2018**, *252*, 128–136, doi:10.1016/j.jmatprotec.2017.09.020.
23. Li, F.; Chen, S.; Shi, J.; Tian, H.; Zhao, Y. Evaluation and Optimization of a Hybrid Manufacturing Process Combining Wire Arc Additive Manufacturing with Milling for the Fabrication of Stiffened Panels. *Appl. Sci.* **2017**, *7*, 1233, doi:10.3390/app7121233.
24. Frazier, W. E. Metal additive manufacturing: A review. *J. Mater. Eng. Perform.* 2014, *23*.
25. Tabernero, I.; Paskual, A.; Álvarez, P.; Suárez, A. Study on Arc Welding Processes for High Deposition Rate Additive Manufacturing. *Procedia CIRP* **2018**, *68*, 358–362, doi:10.1016/J.PROCIR.2017.12.095.
26. Selvi, S.; Vishvaksenan, A.; Rajasekar, E. Cold metal transfer (CMT) technology - An overview. *Def. Technol.* **2018**, *14*, 28–44, doi:10.1016/j.dt.2017.08.002.
27. Ding, J.; Colegrove, P.; Mehnen, J.; Ganguly, S.; Almeida, P. M. S.; Wang, F.; Williams, S. Thermo-mechanical analysis of Wire and Arc Additive Layer Manufacturing process on large multi-layer parts. *Comput. Mater. Sci.* **2011**, *50*, 3315–3322, doi:10.1016/j.commatsci.2011.06.023.
28. Prado-Cerqueira, J. L.; Diéguez, J. L.; Camacho, A. M. Preliminary development of a Wire and Arc Additive Manufacturing system (WAAM). *Procedia Manuf.* **2017**, *13*, doi:10.1016/j.promfg.2017.09.154.
29. González, J.; Rodríguez, I.; Prado-Cerqueira, J.-L.; Diéguez, J. L.; Pereira, A. Additive manufacturing with GMAW welding and CMT technology. *Procedia Manuf.* **2017**, *13*, 840–847, doi:10.1016/J.PROMFG.2017.09.189.
30. Santos, E. C.; Shiomi, M.; Osakada, K.; Laoui, T. Rapid manufacturing of metal components by laser forming. *Int. J. Mach. Tools Manuf.* **2006**, *46*, 1459–1468, doi:10.1016/j.ijmachtools.2005.09.005.
31. Pickin, C. G.; Williams, S. W.; Lunt, M. Characterisation of the cold metal transfer (CMT) process and its application for low dilution cladding. *J. Mater. Process. Tech.* **2010**, *211*, 496–502, doi:10.1016/j.jmatprotec.2010.11.005.
32. Fronius CMT – Cold Metal Transfer: the cold welding process for premium quality Available online: http://www.fronius.com/en/welding-technology/our-expertise/welding-processes/cmt (accessed on Jun 29, 2018).
33. Anwar, M. S.; Untawale, S. P. Measuring the process efficiency of controlled welding processes. *Int. J. Instrumentation, Control Autom.* **2012**, *1*, 33–39.
34. Fronius CMT Advanced: A higher deposition rate, better gap-bridging ability and higher stability Available online: http://www.fronius.com/en/welding-technology/our-expertise/welding-processes/cmt-advanced (accessed on Jun 29, 2018).
35. ISO 6506-1:2014. Metallic materials. Brinell hardness test. Part 1: Test method. International Standards Organisation, Geneva (Switzerland).
36. ISO 18265:2013. Metallic materials - Conversion of hardness values. International Standards Organisation, Geneva (Switzerland).
37. ASTM A370:2017. Standard Test Methods and Definitions for Mechanical Testing of Steel Products. American Society for Testings and Materials, Philadelphia (USA).
38. SAE J417:1983. Hardness tests and hardness number conversions. SAE International, USA.
39. ASME SFA 5.18, Guide to AWS specification for carbon steel electrodes and rods for gas shielded arc welding, American Society of Mechanical Engineers, New York, 2017.
40. ASME SA-36, Specification for carbon structural steel, American Society of Mechanical Engineers, New

York, 2017.

41. ASME SA-285, Specification for pressure vessels plates, carbon steel, low –and intermediate- tensile strength, American Society of Mechanical Engineers, New York, 2017.
42. ASME SA-515, Specification for pressure vessels plates, carbon steel, low –and intermediate- and higher temperature service, American Society of Mechanical Engineers, New York, 2017.
43. ASME SA-516, Specification for pressure vessels plates, carbon steel, for moderate –and lower-temperature service, American Society of Mechanical Engineers, New York, 2017.
44. Liberini, M.; Astarita, A.; Campatelli, G.; Scippa, A.; Montevecchi, F.; Venturini, G.; Durante, M.; Boccarusso, L.; Minutolo, F. M. C.; Squillace, A. Selection of Optimal Process Parameters for Wire Arc Additive Manufacturing. *Procedia CIRP* **2017**, *62*, 470–474, doi:10.1016/j.procir.2016.06.124.
45. *Kobe steel welding handbook*; Kobe steel Ltd, 2014;